A THEORETICAL STUDY OF THE NITRATION OF EUGENOL WITH THE NITRONIUM ION

Ricardo UGARTE[a], Guillermo SALGADO[b,*] and Luis BASÁEZ[c]

[a] *Instituto de Química, Facultad de Ciencias, Universidad Austral de Valdivia, Valdivia, Chile; e-mail: rugarte@uach.cl*

[b] *Departamento de Ciencias Químicas, Facultad de Ciencias Exactas, Universidad Andrés Bello, Sede Concepción, Chile; e-mail: gsalgado41@gmail.com*

[c] *Facultad de Ciencias Químicas, Universidad de Concepción, Concepción, Chile; e-mail: lbasaez@udec.cl*

Received August 6, 2011
Accepted October 26, 2011
Published online December 20, 2011

The nitration of eugenol was investigated by using density functional theory (DFT) calculations. Potential energy surface and molecular electrostatic potential of eugenol was constructed in order to find, respectively, the minimum energy conformers and the possible sites for electrophilic attack. Stationary points were located and characterized at the B3LYP/6-311++G(2d,2p) level of theory. A strongly bound π-complex was found, in which the distance between the nitrogen atom of the NO_2 moiety and the C_1 carbon atom of the aromatic ring is 2.15 Å in the gas phase and 2.06 Å in dichloromethane. The most favorable σ-complex or Wheland intermediate is the result from the interaction between the nitrogen and the C_6 ring carbon atom. The transition state that connects both complexes is more resembling the σ-complex. The nitronium ion exothermically reacts with eugenol to give the π-complex without an energy barrier. The next stage of the reaction pathway, π-complex → σ-complex, is endothermic and involves a Gibbs energy of activation of 7.9–8.0 kcal mol^{-1} (gas phase) and 8.3–8.9 kcal mol^{-1} (CH_2Cl_2).

Keywords: Density functional calculations; Molecular modeling; Quantum chemistry; Eugenol; Nitronium ion; Nitration; π-complex; DFT calculations; Molecular electrostatic potential (MEP).

Eugenol (4-Allyl-2-methoxyphenol), is a yellow oily liquid soluble in alcohol, but exhibiting low solubility in water (Fig. 1)[1]. Therapeutic benefits of eugenol are well known in traditional medical practices: antiseptic, antibacterial and analgesic agent[2]. Nowadays, it is reported to participate in photochemical reactions and to possess insecticidal, antioxidant, anti-inflammatory and antitumor activities[3–6]. In a recent paper[7], and as a contribution to possible future applications, the toxicity and antioxidant capacity of eugenol derivatives were evaluated. In this context, the nitration

doi:10.1135/cccc2011156

of eugenol was carried out; this was dissolved in dichloromethane and added to a stirred mixture which contained potassium hydrogen sulfate, sodium nitrate and wet silica. The principal product was 4-allyl-2-methoxy-6-nitrophenol (63.2%) (Fig. 1).

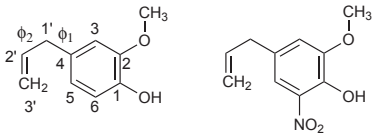

FIG. 1
Eugenol (left) and 6-nitroeugenol (right)

Aromatic nitration is most commonly carried out as an acid-catalyzed reaction between the aromatic substrate and nitric acid[8]. It has been generally accepted that the nitrating agent is the highly reactive nitronium ion, NO_2^+, which is responsible for electrophilic attack on the aromatic compound and that the reaction involves a Wheland intermediate identified as an arenium ion or σ-complex[9–11]. This intermediate in a subsequent step undergoes proton elimination leading to the nitrated product. It was also agreed that the thermodynamic stability of the σ-complex determines the regioselectivity (positional selectivity) of the nitrated products.

$$HNO_3 + HA \rightarrow H_2NO_3^+ + A^- \qquad (1)$$

$$H_2NO_3^+ \rightarrow NO_2^+ + H_2O \qquad (2)$$

$$ArH + NO_2^+ \rightarrow ArHNO_2^+ (\sigma) \qquad (3)$$

$$ArHNO_2^+ (\sigma) \rightarrow ArNO_2 + H^+ \qquad (4)$$

However, in order to explain the low substrate selectivity observed in the nitration of aromatics with the nitronium salts (like nitronium tetrafluoroborate), a modification of the original mechanism was proposed. The observed low substrates selectivities were all accompanied by no alteration in regioselectivity (typical isomer distributions of nitrotoluenes (%) were ortho:meta:para = 66:3:31)[12,13]. As an explanation, the existence of an intermediate, π-complex, prior to the formation of the σ-complexes (for the ortho, meta, para isomers) was suggested. This initial intermediate was con-

sidered a weakly bound state involving low, nonspecific, attractive interaction between the nitronium ion and the aromatic π-system as an entity. Thus, the observed low substrate, but high positional selectivity suggests that substrate selectivity is determined in an early π-complex, followed by the formation of σ-complexes determining regioselectivity.

$$\mathrm{ArH} + \mathrm{NO_2^+} \rightarrow \mathrm{ArH\text{-}NO_2^+}\ (\pi) \qquad (3a)$$

$$\mathrm{ArH\text{-}NO_2^+}\ (\pi) \rightarrow \mathrm{ArHNO_2^+}\ (\sigma) \qquad (4a)$$

$$\mathrm{ArHNO_2^+}\ (\sigma) \rightarrow \mathrm{ArNO_2} + \mathrm{H^+} \qquad (5a)$$

The easy deprotonation of the Wheland intermediate has always been considered to be a fast process, due to the lack of a deuterium isotope effect, and the fact that added bases do not accelerate the reaction. Therefore, the relevant aspects of the electrophilic aromatic nitration mechanism implicate the study of the aforementioned complexes.

In this paper, we report the results of the computational study of the interaction between NO_2^+ ion and eugenol. Our objective was to characterize the intermediate steps through which this reaction may proceed. In this way, we try to rationalize the experimental results obtained in relation to the regioselectivity of the nitration.

Basically, the calculations include: a systematic search on the potential energy surface (PES) of eugenol molecule in order to find the most stable conformers[14], the molecular electrostatic potentials (MEP) of eugenol that allows to study the possible sites of the electrophilic attack of the nitronium ion[15] and finally, to obtain all the stationary points, including transition states (TS), along the reaction path[10,11,13,16–18]. The properties of the π-complexes, σ-complexes and TS will be discussed in detail.

METHODS

All calculations were performed at RHF/6-31G(d), B3LYP/6-311++G(2d,2p) and B3LYP/SV(P) levels of theory by using, Gaussian 03 and ORCA computer programs[19,20] running on a Dell PowerEdge R805 server.

The linear nitronium ion was optimized at B3LYP/6-311++G(2d,2p) level. In order to construct the potential energy surface (PES) of eugenol, the restricted Hartree–Fock (RHF) ab initio procedure with the standard 6-31G(d) basis set was employed. These calculations are relatively inexpensive in

computational terms and yield reasonable structural data. Starting from an input structure[14], with the methoxy and hydroxyl groups in the plane of the benzene ring, the PES was constructed by varying the dihedral angles Φ_1 and Φ_2 (Fig. 1); these angles determine the possible conformations of the molecule. The dihedral angle Φ_1 of the bonded atoms C_3–C_4–$C_{1'}$–$C_{2'}$ is the angle between the planes C_3–C_4–$C_{1'}$ and C_4–$C_{1'}$–$C_{2'}$. Viewed from the direction of C_3, Φ_1 is positive for clockwise and negative for anticlockwise rotations. Thus, the value $\Phi_1 = 0°$ corresponds to the planar cis-arrangement of the bonds C_3–C_4 and $C_{1'}$–$C_{2'}$, while the value $\Phi_1 = 180°$ corresponds to the planar trans-arrangement. The PES was calculated using a 19 × 19 grid generated by rotating through Φ_1 and Φ_2 in 20° increments from –180 to +180°. At each point, a complete geometry optimization was performed with Φ_1 and Φ_2, frozen at their respective grid values. Conformational energy map (contour diagram) was drawn in order to facilitate the analysis of the data. Unconstrained geometry optimizations (full optimizations) at the B3LYP/6-311++G(2d,2p) level were performed with a set of initial conformations, chosen to lie close to the minima found on the PES. As from the previous result, the optimized structures of the minimum energy conformers were obtained.

Contour diagrams of the MEP have been employed for understanding the reactivity between both molecules. Briefly, the electrostatic potential represents the effects of the nuclei and the electrons; in those regions where the electrostatic potential is negative, the contribution of the electrons predominates and it is there that an electrophile is initially attracted, particularly to the point at which occurs the most negative value of the electrostatic potential[15] occurs. In order to evaluate the molecular electrostatic potential of eugenol we have used the Cubegen utility implemented in Gaussian 03.

The nitronium ion and the eugenol molecule were brought together with their both relative orientations and the aromatic carbon–nitrogen distance being restricted. Since the eugenol is not symmetric, the attack of the ion is carried out on both sides of the ring (front and back side). The distance between the nitrogen atom of the nitronium ion and the attacked aromatic carbon atom was chosen as the reaction coordinate. The approximation of NO_2^+ ion is parallel to the plane of the aromatic ring and the angle N–C[3, 5 or 6]–C[Ar] = 90°. This relaxed scan procedure, followed by the full optimization of the minima, was found useful to produce the π-complexes in which the ion is located well above the aromatic ring. The σ-complexes were easily obtained by placing the NO_2^+ ion (at an appropriate bond distance) to the ring carbon (3, 5 or 6) and performing a full geometry optimi-

zation. Next, we proceeded to find the TS structures that connect both complexes; in addition, intrinsic reaction coordinate (IRC) analysis was carried out for each transition state to make sure that the π-complex and the σ-complex are connected to the transition structure obtained.

Since the reaction takes place in a solution, we have explored the solvent effects by using the polarizable continuum model (PCM) implemented in the Gaussian 03 program. Even though the nitration medium is very complex, we thought that in the reaction possibly the characteristics or properties of dichloromethane (CH_2Cl_2, dielectric constant ≈ 9) predominate. The above could be justified owing to the low solubility of eugenol and dichloromethane in aqueous solution.

Vibrational frequency calculations were carried out to confirm the nature of all stationary points: local minima had no negative (imaginary) frequency; saddle points had exactly one imaginary frequency.

In general, the ORCA program was only used to locate the stationary points of the NO_2^+–eugenol system submitted to restrictions on internal coordinates; these calculations were performed at B3LYP/SV(P) level of theory. Full optimization of the structures obtained in the previous stage was performed at the B3LYP/6-311++G(2d,2p) level using the Gaussian 03 program.

RESULTS AND DISCUSSION

Eugenol

The conformational energy map of eugenol is shown in Fig. 2. The global minimum A is located approximately at $[\Phi_1, \Phi_2] = [\pm 60°, \mp 120°]$ (a pair of mirror images). The local minima B, C are situated approximately at $[\Phi_1, \Phi_2] = [\pm 120°, \pm 120°]$ and $[\pm 75°, 0°]$, respectively. Full optimization (B3LYP/6-311++G(2d,2p)) of the structures located at these regions was performed. Thus, the lowest-energy conformers of eugenol were obtained. All conformers are stabilized by intramolecular hydrogen bond between the –OH donor and $–OCH_3$ acceptor groups, and the population abundance of these structures is approximately 99.8%: A (47.9%), B (41.2%) and C (10.7%). The remaining structures (0.2%) also show both groups in the plane of the benzene ring, but in the configurations, where the hydrogen bonding is not possible[14].

The candidates to perform the nitration analysis are the A (global minimum) and B conformers. However, since the rotational barrier between A

and B conformers in relation to Φ_1 is not large, approx. 8 kcal mol^{-1} or less (Fig. 2), free rotation exists around of this dihedral angle at ambient temperature. For simplicity, we have chosen the global minimum (Fig. 3). In addition, the electrophilic attack modifies the structure (Φ_1 and Φ_2 dihedral angles) of eugenol; therefore, it is probable that the interaction of the nitronium ion with B conformer yield the same complex generated between the global minimum and the nitronium ion.

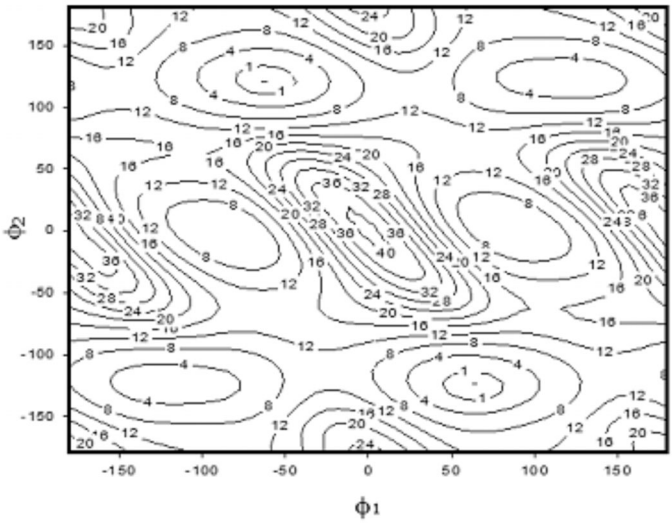

FIG. 2
Conformational energy map of eugenol [RHF/6-31G(d)]. ΔE_{HF} are in kcal mol^{-1} with respect to the global minimum

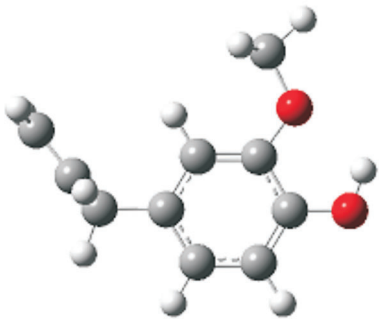

FIG. 3
The eugenol molecule optimized at B3LYP/6-311++G(2d,2p) level

Molecular Electrostatic Potential of Eugenol

The molecular electrostatic potential is an effective guide for interpreting and predicting the molecular interactions. The electrostatic potential, that is created in the space around a molecule by its nuclei and electrons, is a useful analytical tool in the study of molecular reactivity[21]. It is through this potential that a molecule is first "seen" or "felt" by an approaching chemical species; therefore, is very valuable in the study of electrophilic processes. Thus, an approaching electrophile will initially be attracted to those regions in which the MEP is negative, and in particular to the points where the electrostatic potential has its most negative values (the local minima).

Figures 4 and 5 show the MEP of eugenol. The molecule presents the same orientation as in Fig. 3. The contour lines are plotted as a function of the distance to the plane passing through the aromatic ring. For clarity, the MEP in the plane of the ring is shown; thus, it is possible to identify the most important atomic positions.

In Fig. 4a, the *a* value (approx. –18 kcal mol^{-1}) related with the oxygen of the –OH group, can be attributed to the effect of its lone pair; while the *b* value (approx. –16 kcal mol^{-1}) is interpreted as being due to the π-electron cloud of the aromatic ring. The negative potentials associated to *c* and *d*, *e* are due to methoxy oxygen and carbon 3′ of the allyl group, respectively. In a larger distance of the plane of the ring (Fig. 4b), the negative *a–b* region continues being important. Figures 5a and 5b show an analogous pattern to the above figures, except for the absence of the effect produced by the allyl group (*d* and *e* regions).

The negative region *a–b* is a highly favorable site for electrophilic attack. The minimal values of potential are reached at this region and by contrast to the other regions always remain "visible" for the electrophile.

It is interesting to note that the linear NO_2^+ (2.24 Å in length) can be accommodated along the *a–b* axis (≈ 3 Å). The driving property of the MEP becomes important for the progress of the reaction; in particular, the ion attack will have high probabilities of being directed towards the ring's carbon atoms close to the region of minimum electrostatic potential. In consequence, the process driven by the MEP would be able to determine the regioselectivity of the reaction, especially if the stabilization of nitronium ion is indeed achieved through the formation of a π-complex. Thus, this complex should determine the features of the Wheland intermediate.

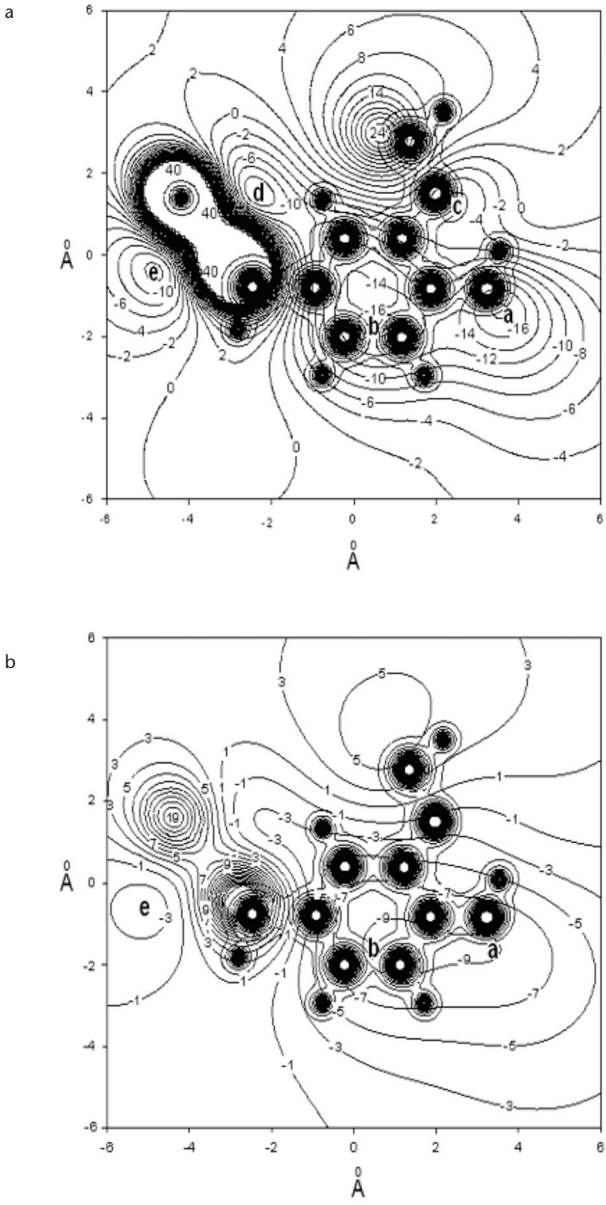

FIG. 4
MEP of eugenol at B3LYP/6-311++G(2d,2p) level in the plane 2.00 Å (a) and 3.00 Å (b) above the ring plane. The position of the ring is shown. Potential minima (in kcal mol^{-1}) occur at points indicated by lower cases. $C_1 \approx [2, -1]$

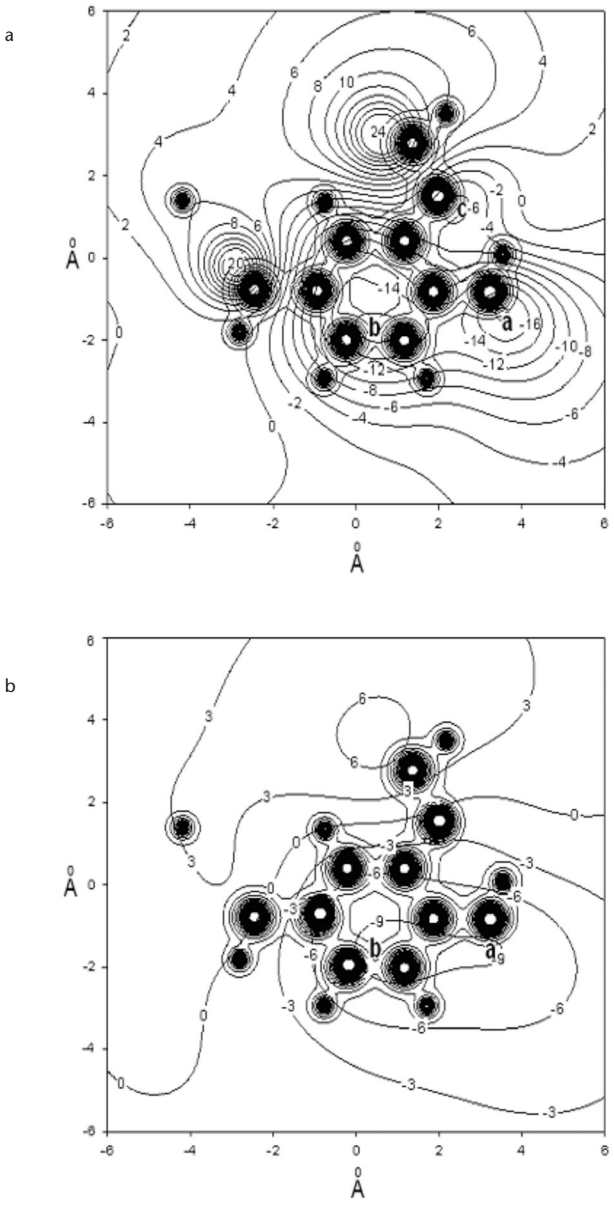

FIG. 5
MEP of eugenol at B3LYP/6-311++G(2d,2p) level in the plane 2.00 Å (a) and 3.00 Å (b) below the ring plane. The position of the ring is shown. Potential minima (in kcal mol^{-1}) occur at points indicated by lower cases. $C_1 \approx [2, -1]$

Reaction of the Eugenol Molecule with the Nitronium Ion

The linear nitronium ion can interact with the eugenol molecule (Fig. 3) either from above or below the plane of ring (front-side or back-side attack). In all calculated complexes, the linear nitronium ion changes towards a bent structure. Table I lists the data of all optimized structures at the B3LYP/6-311++G(2d,2p) level of theory that are pertinent to this study (Figs 6 and 7).

π-*Complexes*. The MEP suggests that the *a–b* region is a good site for electrophilic attack. Effectively, this is demonstrated by the two calculated complexes; to compare f-π_1 (Fig. 6) with Fig. 4a, and b-π_1 (Fig. 7) with Fig. 5a.

As the nitronium ion approaches to the *a–b* region, the O–N–O angle becomes more acute with the two oxygen atoms moving away from the ring; this angular deformation demonstrates the interaction with eugenol. The calculated structures should be characterized as π-complexes due to the fact that the interaction of the nitronium ion with the π-system practically does

TABLE I
B3LYP energies, Mulliken's charges and relevant structural properties of the stationary points

Specie[a]	Bond length[b]	Energy[c]	Stabilization energy[d]	NO_2 Moiety		Dihedral angles	
				Atomic charge[e]	O–N–O Angle	C_3–C_4–C_1–$C_{2'}$	C_4–C_1–C_2–$C_{3'}$
N-E		–743.660210	0	1.000	180.0	–58.2	122.4
f-π_1	2.15	–743.752555	–58.0	0.189	134.5	–17.1	117.1
f-σ_3	1.65	–743.738128	–48.9	–0.012	129.2	–59.7	118.8
f-σ_5	1.64	–743.754143	–58.9	–0.068	128.8	–20.0	115.3
f-σ_6	1.59	–743.744344	–52.8	–0.051	128.9	–59.2	119.0
f-TS_6	2.02	–743.740989	–50.7	0.219	135.3	–60.9	120.1
b-π_1	2.15	–743.752679	–58.0	0.197	134.5	–19.8	116.8
b-σ_3	1.58	–743.742171	–51.4	–0.052	128.0	–70.6	115.3
b-σ_5	1.58	–743.754325	–59.1	–0.046	128.1	–21.2	116.1
b-σ_6	1.59	–743.744139	–52.7	–0.074	129.0	–60.0	119.1
b-TS_6	2.00	–743.741070	–50.7	0.218	135.2	–58.1	119.5

[a] See Figs 6 and 7. [b] Between the nitrogen atom and the ring carbon atom indicated in the number found in the notation (Å). [c] Energy values are in a.u. [d] Energy values relative to the separated reactants (N-E) are in kcal mol^{-1}. [e] Values are in electron units. Angles are in degrees

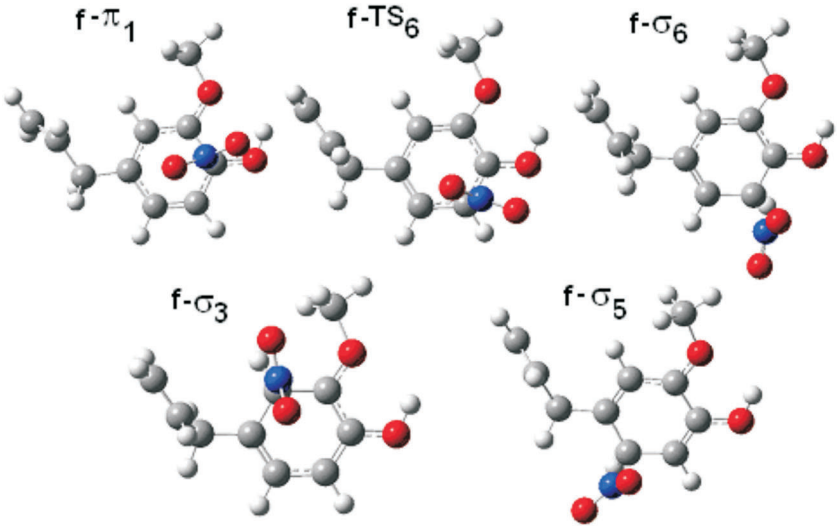

FIG. 6
Structure and label of the stationary points optimized at B3LYP/6-311++G(2d,2p) level

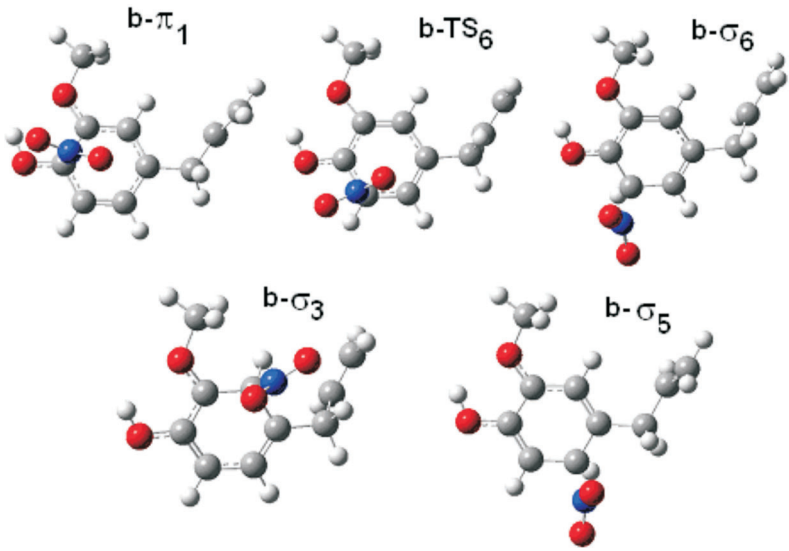

FIG. 7
Structure and label of the stationary points optimized at B3LYP/6-311++G(2d,2p) level

not distort the aromatic ring (the sp^2 hybridization of the C_1 carbon atom is maintained). The stabilization energy of the π-complexes is quite high, since the dispersion of the positive charge over the whole system yields greater stability. An analysis of the redistribution of the Mulliken charges indicates that the electronic charge migration from the eugenol to the nitronium ion takes place through the following groups: $–OCH_3$, allyl, –OH and aromatic hydrogens; the group of the ring carbons practically does not vary its charge. In these complexes, the nitronium ion charge is approx. 0.2 electron units and the O–N–O angle (≈ 134.5°) tends to get close to the angle of the paramagnetic completely reduced nitrogen dioxide (134.3°)[22]. Thus, from a strictly structural point of view, the nitronium ion suffers a one-electron reduction at the expense of eugenol.

In order to investigate approximately the bond character of the π-complex, a charge decomposition analysis (CDA)[23] was carried out at the B3LYP/6-31G(d,p) level of theory, with the complexes optimized on the same level (the basis set 6-311++G(2d,2p) gave unrealistic results). The CDA shows that there is a small amount of charge, approx. 0.18 electron units, donated from eugenol into the bonding region (covalent interaction), while the electronic charge back donation from the NO_2^+ moiety is negligible. However, the net Mulliken charge transfer from the eugenol molecule towards nitronium ion is approx. 0.98 electron units. Thus, probably the electrostatic attractions are the source of the principal bonding interactions.

σ-*Complexes*. In these bound systems, the NO_2 moiety is localized at a single carbon atom, such as C_3, C_5 or C_6. The interaction causes that the involved carbon atoms to "rehybridise" from sp^2 towards sp^3. The structures of these intermediate carbocations reflect the partial loss of aromatic character; the NO_2-bearing carbons are quasi-tetrahedral and the hydrogen atoms attached to these carbon atoms are shifted out of the ring plane (Figs 6 and 7). The O–N–O angles are between 127.9 and 129.3° and corroborate the complete reduction of nitronium ion; thus, in these complexes there is a very sizable transfer of electronic charge from the eugenol molecule to the nitronium ion (1.04–1.08 electron units), whose charge is more than neutralized (Table I).

According to the stabilization energies, the order of stability of the complexes is f(b)-σ_3 < f(b)-σ_6 < f(b)-σ_5. From an energetic point of view, the formation of the f(b)-σ_5 complexes would be favored (product stability principle), which constitutes an evident contradiction with the facts, because the preferred site for the electrophilic attack of the nitronium ion is

at C_6 position of the eugenol. The above can be explained if we considered the driving property of the MEP, just as it has been indicated at the last paragraph of Molecular Electrostatic Potential of Eugenol. Thus, owing to the previous step that involve to the π-complex, the most probable site for the subsequent formation of Wheland intermediate is at C_6, i.e., the closer site to the C_1 aromatic carbon.

By invoking the principle of least motion[24], it is also possible to justify the formation of the f(b)-σ_6. Like the product stability principle, the principle of least motion deals with reactivity in the terms of reactant(s) and product(s) of the reaction and, it is composed of two parts: the principle of least nuclear motion and the principle of least change in electronic configuration. In this way, if we apply the first part of the principle, the reaction that yields f(b)-σ_6 will be favored, since, in respect of the other ones, involve the least change in atomic positions (Fig. 8). In fact, if we compared the values of the dihedral angles of the σ-complexes listed in Table I, the f-σ_6 and b-σ_6 are structurally the most resembling to the eugenol molecule (the f-σ_3 complex evidences a severe distortion of the aromatic ring).

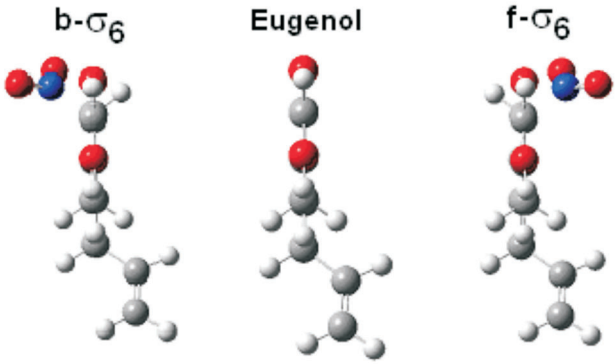

FIG. 8
Illustration of the principle of least motion: except for the top hydrogen atom, the eugenol molecule remains practically invariable. The above is not applicable to the other σ-complexes

The reaction path. Table II lists the thermochemical data of the most relevant complexes. It is evident that these are much more stable than the separated reactants (N-E). Therefore, their formation is highly favored, consistent with the fact that the NO_2^+ interacts strongly with electron-rich aromatic compounds. According to our calculations, the reaction of eugenol with the nitronium ion to yield the π-complex is exothermic

(–57.6 kcal mol^{-1}) and no energy barrier is involved; the driving force for the reaction is of enthalpic nature. The next step, π-complex → σ-complex, is endothermic (6.6–6.8 kcal mol^{-1}); the Gibbs energy of activation for this reaction is 8.0–7.9 kcal mol^{-1}.

At the transition state, the distance N–C_1 ≈ 2.5 Å, while the distance N–C_6 ≈ 2.0 Å; therefore, f(b)-TS_6, in respect to the nitrogen atom, is approximately equidistant of both complexes. Nevertheless, if we consider the di-

TABLE II
Thermochemical data[a] of the Pertinent structures at B3LYP/6-311++G(2d,2p) level of theory with zero-point energy (ZPE) corrections

Specie	ΔH^0	ΔS^0	ΔG^0	$\Delta(\Delta H^0)$	$\Delta(\Delta S^0)$	$\Delta(\Delta G^0)$
N-E	0	0	0			
f-π_1	–57.6	–35.0	–47.2	0	0	0
f-TS_6	–50.6	–37.9	–39.2	7.0	–2.9	8.0
f-σ_6	–51.0	–35.7	–40.3	6.6	–0.7	6.9
b-π_1	–57.6	–35.5	–47.0	0	0	0
b-TS_6	–50.5	–38.2	–39.1	7.1	–2.7	7.9
b-σ_6	–50.8	–36.0	–40.0	6.8	–0.5	7.0

[a] At 298.15 K, 1 atm. The energy values are in kcal mol^{-1} and the entropy values are in cal K^{-1} mol^{-1}. Δ: Relative to the separated reactants (N-E). Δ(Δ): Relative to the correspondent π-complex

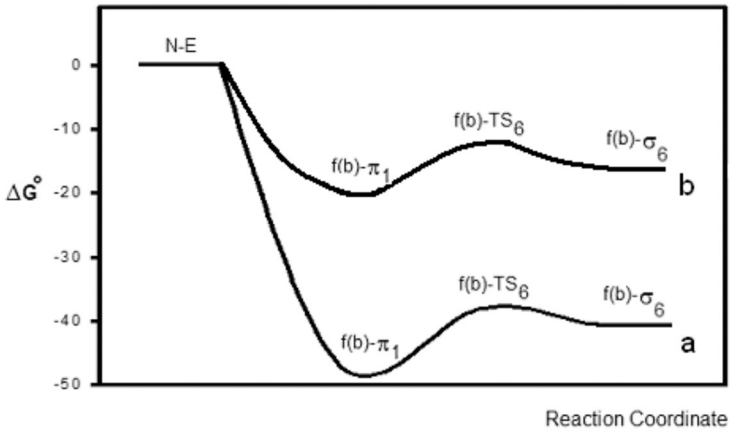

FIG. 9
Scheme of the reaction profile: gas phase (a) and dichloromethane (b). ΔG^0 are in kcal mol^{-1}

hedral angles (Table I), the transition state is more closely resembling the σ-complex than the π-complex. Hence, according to the Hammond postulate, it is fulfilled that π-complex → σ-complex reaction is endothermic, because TS ↔ σ-complex interconversion involve only a small reorganization of the molecular structure[25].

A possible reaction path is shown in Fig. 9, where the general exergonicity of the reaction is evident and the transition state and the σ-complex or Wheland intermediateare are close in the energy content.

Solvent Effects

The solvent effect (Table III) results in the decrease of the energy of the system. The separated reactants have a higher stabilization energy by solvent (ΔE_s = E(specie)$_{CH2Cl2}$ – E(specie)$_{gas\ phase}$) than the complexes, because the latter already have exerted a stabilizing effect in gas phase by dispersing the ionic charge over the whole system. The ΔE_s of eugenol is –3.5 kcal mol^{-1} and ΔE_s of nitronium ion is –64.7 kcal mol^{-1}; i.e., the stabilization of NO_2^+ is the main effect of dichloromethane. Thus, the formation of the complexes in CH_2Cl_2 evolves less energy that in the gas phase (Table IV). The reaction in dichloromethane environment has an energy profile analogous to the reaction in gas phase (Fig. 9).

TABLE III
B3LYP Energies and relevant structural properties of the Pertinent stationary points in CH_2Cl_2

Specie[a]	Bond length[b]	Energy[c]	Stabilization energy[d]	ΔE_s[e]	Angle O–N–O	Dihedral angles	
						C_3–C_4–C_1–$C_{2'}$	C_4–C_1–$C_{2'}$–$C_{3'}$
N-E		–743.768830	0	–68.2	180.0	–65.1	122.5
f-π_1	2.06	–743.817433	–30.5	–40.7	131.8	–11.2	118.2
f-TS_6	2.08	–743.805132	–22.8	–40.2	134.5	–68.0	119.2
f-σ_6	1.55	–743.814698	–28.8	–44.2	127.1	–62.6	117.7
b-π_1	2.06	–743.817415	–30.5	–40.6	132.0	–13.1	117.7
b-TS_6	2.08	–743.805156	–22.8	–40.2	134.6	–62.7	118.7
b-σ_6	1.55	–743.814580	–28.7	–44.2	127.1	–64.3	118.8

[a] See Figs 6 and 7. [b] Between the nitrogen atom and the ring carbon atom indicated in the number found in the notation (Å). [c] Energy values are in a.u. [d] Energy values relative to the separated reactants (N-E) are in kcal mol^{-1}. [e] ΔE_s = E(specie)$_{CH2Cl2}$ – E(specie)$_{gas\ phase}$. Angles are in degrees

TABLE IV
Thermochemical data[a] at B3LYP/6-311++G(2d,2p) level of theory in CH_2Cl_2 (ZPE corrections)

Specie	ΔH^0	ΔS^0	ΔG^0	$\Delta(\Delta H^0)$	$\Delta(\Delta S^0)$	$\Delta(\Delta G^0)$
N-E	0	0	0			
f-π_1	–30.2	–35.6	–19.6	0	0	0
f-TS_6	–22.8	–38.6	–11.3	7.4	–3.0	8.3
f-σ_6	–26.6	–35.6	–16.0	3.6	0	3.6
b-π_1	–30.4	–33.9	–20.3	0	0	0
b-TS_6	–22.8	–38.2	–11.4	7.6	–4.3	8.9
b-σ_6	–26.4	–36.9	–15.4	4.0	–3.0	4.9

[a] At 298.15 K, 1 atm. The energy values are in kcal mol^{-1} and the entropy values are in cal K^{-1} mol^{-1}. Δ: Relative to the separated reactants (N-E). Δ(Δ): Relative to the correspondent π-complex

The dichloromethane has only a slight effect on the MEP of eugenol (Fig. 10). The MEP values in the region of interest exhibits a small increase with respect to the gas-phase values; the immediate effect of such variation is to reduce a little the N–C_1 bond length in the π-complexes.

Condensed Fukui Functions

The condensed Fukui functions[26,27] are quantum chemical descriptors widely used to probe the reactive sites in a molecule. The atom with the highest condensed Fukui function is the most reactive compared to other atoms in the molecule.

The B3LYP/6-311++G(2d,2p) selected structures to perform the calculations are eugenol and the eugenol moiety obtained from the corresponding complex or TS. In Table V, condensed Fukui function values are presented for an electrophilic attack (f_k-), for C_3, C_5 and C_6 atoms. The calculations were carried out at the B3LYP/6-31G(d) level of theory, because 6-311++G(2d,2p) basis set gave unrealistic results. Commonly, the condensed Fukui functions are calculated for the reactant (eugenol), and from this point of view, the obtained values fail as predictors of site reactivity: $C_5 > C_6 > C_3$. Nevertheless, it is interesting to note that the appropriate order of the site reactivity is fulfilled as the eugenol molecule tends to assume the structure of the final stage of the process.

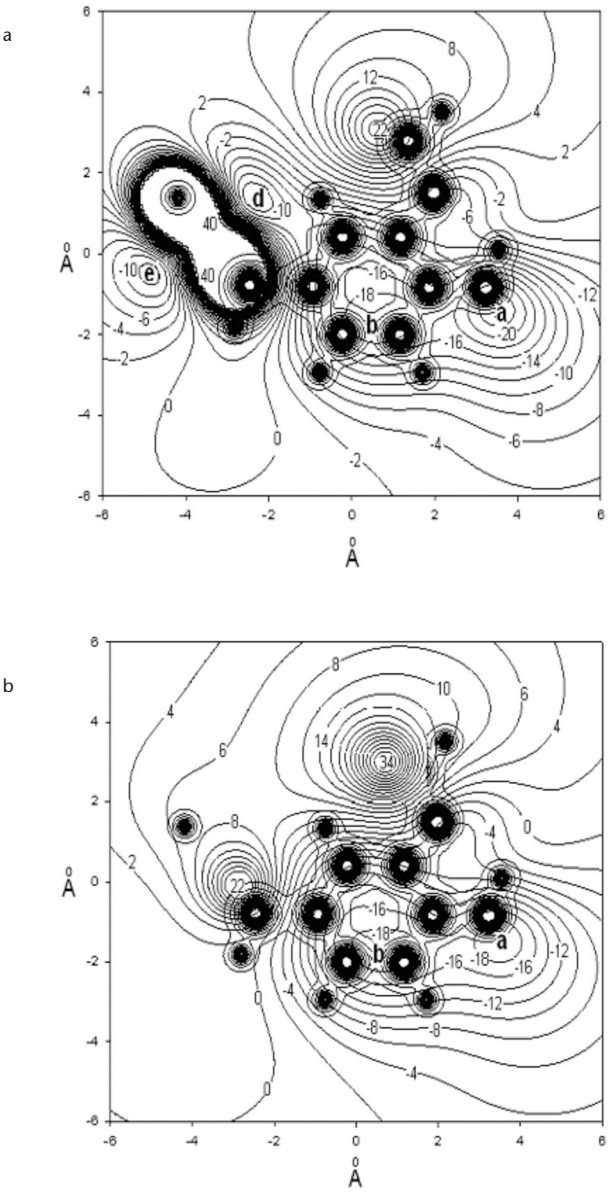

FIG. 10
MEP of eugenol in CH_2Cl_2 at B3LYP/6-311++G(2d,2p) level in the plane 2.00 Å above the ring plane (a) and 2.00 Å below the ring plane (b). The position of the ring is shown. Potential minima (in kcal mol^{-1}) occur at points indicated by lower cases. $C_1 \approx [2, -1]$

TABLE V
The condensed Fukui functions for an electrophilic attack at B3LYP/6-31G(d)//B3LYP/6-311++G(2d,2p) level of theory

Specie[a]	Gas phase			CH_2Cl_2		
	f_k-C_3	f_k-C_5	f_k-C_6	f_k-C_3	f_k-C_5	f_k-C_6
E	0.002	0.119	0.054	0.004	0.134	0.044
E → f-π_1	0.003	0.115	0.045	0.004	0.121	0.040
E → f-TS_6	0.009	0.069	0.133	0.005	0.082	0.116
E → f-σ_6	0.029	0.027	0.281	0.031	0.024	0.333
E → b-π_1	0.003	0.115	0.046	0.004	0.125	0.040
E → b-TS_6	0.009	0.069	0.134	0.005	0.082	0.115
E → b-σ_6	0.027	0.028	0.278	0.029	0.024	0.336

[a] E or eugenol. E → represents the eugenol moiety obtained as from the respective complex or TS

CONCLUSIONS

This account reports the theoretical results of the systematic investigation of some possible intermediate stages in the nitration of eugenol. Our intention in this work was to attempt to justify the experimental fact that the nitration occurs mainly at the C_6 atom of the aromatic ring. In this sense, the molecular electrostatic potential of eugenol fulfills a crucial role, because it governs the reactivity during the initial stage of reaction, leading to the formation and stabilization of the key intermediate[28] or π-complex that orientate the subsequent formation of the Wheland intermediate. Thus, by virtue of a "notion of proximity", the C_1 atom of the π-complex involves the posterior participation of the C_6 atom in the σ-complex; i.e., the regioselectivity is determined by the π-complex. Finally, another justification for the preferred formation of the f(b)-σ_6 complexes comes from the principle of least motion.

In the near future, we will try to inquire in the electron transfer mechanism[29,30] of the nitration of eugenol: SET or polar pathway?

The authors wish to acknowledge the DID-UACH (Grant S-2008-26) for financial support, and to Dr Lorena Gerli Candia for their valuable assistance.

REFERENCES

1. Garza E., Toranzo J. M.: *ADM* **1988**, *55*, 46.
2. Ghosh R., Nadiminty N., Fitzpatrick J. E., Alworth W. L., Slaga T. J., Kumar A. P.: *J. Biol. Chem.* **2005**, *280*, 5812.
3. Mihara S., Shibamoto T.: *J. Agric. Food Chem.* **1982**, *30*, 1215.
4. Park I.-K., Lee H.-S., Lee S.-G., Park J.-D., Ahn Y.-J.: *J. Agric. Food Chem.* **2000**, *48*, 2528.
5. Ogata M., Hoshi M., Urano S., Endo T.: *Chem. Pharm. Bull.* **2000**, *48*, 1467.
6. Yoo C. B., Han K. T., Cho K. S., Ha J., Park H. J., Nam J. H., Kil U. H., Lee K. T.: *Cancer Lett.* **2005**, *225*, 41.
7. Hidalgo M., De la Rosa C., Carrasco H., Cardona W., Gallardo C., Espinoza C.: *Química Nova* **2009**, *32*, 1467.
8. Levin D. E., Lowy A.: *J. Am. Chem. Soc.* **1933**, *55*, 1995.
9. Hughes E. D., Ingold C. K., Reed R. I.: *J. Chem. Soc.* **1950**, 2400.
10. Politzer P., Jayasuriya K., Sjoberg P., Laurence P. R.: *J. Am. Chem. Soc.* **1985**, *107*, 1174.
11. Sokolov A. V.: *Int. J. Quantum Chem.* **2004**, *100*, 1.
12. Olah G. A.: *Acc. Chem. Res.* **1971**, *4*, 240.
13. Esteves P. M., de M. Carneiro J. W., Cardoso S. P., Barbosa A. G. H., Laali K. K., Rasul G., Prakash G. K. S., Olah G. A.: *J. Am. Chem. Soc.* **2003**, *125*, 4836.
14. Olbert-Majkut A., Wierzejewska M.: *J. Phys. Chem. A* **2008**, *112*, 5691.
15. Politzer P., Abrahmsen L., Sjoberg P.: *J. Am. Chem. Soc.* **1984**, *106*, 855.
16. Szabo K. J., Hoernfeldt A. B., Gronowitz S.: *J. Am. Chem. Soc.* **1992**, *114*, 6827.
17. Chen L., Xiao H., Xiao J., Gong X.: *J. Phys. Chem. A* **2003**, *107*, 11440.
18. Queiroz J. F. d., Carneiro J. W. d. M., Sabino A. A., Sparrapan R., Eberlin M. N., Esteves P. M.: *J. Org. Chem.* **2006**, *71*, 6192.
19. Frisch M. J., Trucks G. W. S., Schlegel H. B., Scuseria G. E., Robb M. A., Cheeseman J. R., Montgomery J. A., Jr., Vreven T., Kudin K. N., Burant J. C., Millam J. M., Iyengar S. S., Tomasi J., Barone V., Mennucci B., Cossi M., Scalmani G., Rega N., Petersson G. A., Nakatsuji H., Hada M., Ehara M., Toyota K., Fukuda R., Hasegawa J., Ishida M., Nakajima T., Honda Y., Kitao O., Nakai H., Klene M., Li X., Knox J. E., Hratchian H. P., Cross J. B., Bakken V., Adamo C., Jaramillo J., Gomperts R., Stratmann R. E., Yazyev O., Austin A. J., Cammi R., Pomelli C., Ochterski J. W., Ayala P. Y., Morokuma K., Voth G. A., Salvador P., Dannenberg J. J., Zakrzewski V. G., Dapprich S., Daniels A. D., Strain M. C., Farkas O., Malick D. K., Rabuck A. D., Raghavachari K., Foresman J. B., Ortiz J. V., Cui Q., Baboul A. G., Clifford S., Cioslowski J., Stefanov B. B., Liu G., Liashenko A., Piskorz P., Komaromi I., Martin R. L., Fox D. J., Keith T., Al-Laham M. A., Peng C. Y., Nanayakkara A., Challacombe M., Gill P. M. W., Johnson B., Chen W., Wong M. W., Gonzalez C., Pople J. A.: *Gaussian* 03, Gaussian Inc., Wallingford (CT) 2004.
20. Neese F.: *ORCA – An ab initio, Density Functional and Semiempirical Program Package*, v. 2.8-00. Universität Bonn, Bonn 2007.
21. Politzer P., Murray J. S. in: *Reviews in Computational Chemistry* (K. B. Lipkowitz, D. B. Boyd, Eds.), Vol. 2, pp. 273–312. Wiley-VHC, New York 1991.
22. Olbert-Majkut A., Mielke Z., Wieczorek R., Latajka Z.: *Int. J. Quantum Chem.* **2002**, *90*, 1140.
23. Dapprich S., Frenking G.: *J. Phys. Chem.* **1995**, *99*, 9352.
24. Hine J.: *Adv. Phys. Org. Chem.* **1977**, *15*, 1.
25. Hammond G. S.: *J. Am. Chem. Soc.* **1955**, *77*, 334.

26. Fukui K.: *Science* **1982**, *218*, 747.
27. Yang W., Mortier W. J.: *J. Am. Chem. Soc.* **1986**, *108*, 5708.
28. Lenoir D.: *Angew. Chem. Int. Ed.* **2003**, *42*, 854.
29. Shopsowitz K., Lelj F., MacLachlan M. J.: *J. Org. Chem.* **2011**, *76*, 1285.
30. Wang P.-C., Chen J., Ming L.: *J. Chin. Chem. Soc.* **2010**, *57*, 967.